Neutron Inelastic Scattering, Optical Spectroscopies, and Scaled Quantum Mechanical Force Fields for Analyzing the Vibrational Dynamics of Pyrimidine Nucleic Acid Bases. 2. Thymine

A. Aamouche and M. Ghomi*

Laboratoire de Physicochimie Biomoléculaire et Cellulaire, CNRS URA 2056, Case courrier 138, Université Pierre et Marie Curie, 4 Place Jussieu, F75252 Paris Cedex 05, France

C. Coulombeau

Laboratoire d'Etudes Dynamiques et Structurales de la Sélectivité, CNRS URA 332, Université J. Fourier, BP 53X, F-38041 Grenoble, France

L. Grajcar and M. H. Baron

Laboratoire de Spectrochimie Infrarouge et Raman, CNRS UPR 2631, 2 rue H. Dunant, F-94320 Thiais, France

H. Jobic

Institut de Recherche sur la Catalyse, 2 avenue A. Einstein, F-69626 Villeurbanne, France

G. Berthier

Institut de Biologie Physico-Chimique, 13 rue Pierre et Marie Curie, F-75231 Paris Cedex 05, and Laboratoire de Radioastronomie Millimétrique, Ecole Normale Supérieure, F-75231 Paris Cedex 05, France

Received: July 31, 1996; In Final Form: November 11, 1996[⊗]

As in the case of uracil, a complete set of vibrational spectra of thymine and its N-deuterated species, obtained from several spectroscopic techniques, i.e., neutron inelastic scattering (NIS), Raman scattering, and infrared absorption (IR), has been used in order to assign the vibrational modes on the basis of an ab initio scaled quantum mechanical (SQM) force field. NIS, Raman, and IR spectra of polycrystalline thymine recorded at $T = 15$ K provide complementary data for analyzing different groups of molecular vibrational modes. Solid-state spectra have been supplemented with FT Raman ($\lambda_{exc} = 1.06$ μm) and IR spectra of aqueous solutions. The spectra from both phases allowed us to analyze the effects of the environment related to strong (crystal) or weak (solution) hydrogen bondings. The molecular fundamental wavenumbers calculated at the SCF+MP2 level, by using different types of molecular orbitals, have first been compared with the experimental wavenumbers taken from the gas phase of thymine. Then the force field has been scaled in order to improve the agreement with experimental data from solid and aqueous phases. The scaling procedure is similar to that established in the case of uracil. We have used the Pulay method in order to improve the wavenumbers and NIS intensities corresponding to the bond stretchings and angular bendings as well as those related to the methyl group vibrational motions. The majority of these scaling factors lie close to unity (between 0.8 and 1.1), except for the methyl torsion, for which a large value of 1.4 was needed. The other force constants related to the ring torsional and wagging motions have been scaled by the least-squares refinement of the off-diagonal force constant expressed in terms of internal coordinates.

Introduction

In a first paper of this series,[1] we have reported our experimental and theoretical results on the structurally simplest pyrimidine base, i.e., uracil. From the experimental point of view, neutron inelastic scattering (NIS) spectra recorded in the solid phase at low temperature were used to analyze the low wavenumber vibrational modes and especially those in which the hydrogen atoms are involved. The NIS cross section for hydrogen atoms is several times larger than that of the other atoms, so in the NIS process the intensity is largely modulated by hydrogen displacements. NIS spectra were compared with those obtained at low temperature by Raman and IR techniques. Raman and IR spectra of the aqueous solutions were recorded in order to study the effects of environment on the internal modes in going from solid phase (where strong intermolecular H-bonds exist) to solution (where weaker hydrogen bonds are formed with solvent molecules). This new and complete set of experimental spectra, together with the previously published vibrational spectra in gas phase and in rare-gas matrixes, has been used in order to assign as accurately as possible the molecular normal modes by means of the quantum mechanical force field obtained at SCF+MP2 level.

In this work we present our results on thymine (5-methyl-uracil, DNA base) obtained by the experimental and theoretical methodologies already applied to uracil (RNA base).[1] The main aim of the present investigation is to estimate the extent to which the molecular vibrational dynamics is influenced by the presence of a methyl group in the 5 position of the molecular ring.

It should be reminded that in the past, numerous experimental

* To whom correspondence should be addressed.

[⊗] Abstract published in *Advance ACS Abstracts,* February 15, 1997.

S1089-5639(96)02318-3 CCC: $14.00

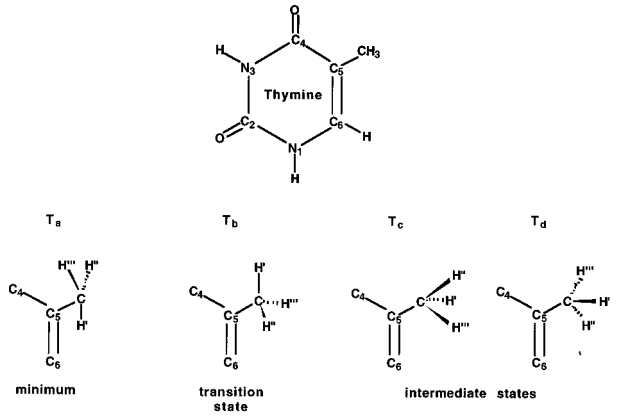

Figure 1. Chemical structure and atom numbering of thymine. The four privileged conformations of the methyl group named T_a, T_b, T_c, and T_d are also reported in the lower part of this figure.

investigations have been devoted to vibrational analysis of thymine using optical spectroscopies: in the gas phase,[2] in Ar matrix,[3,4] in the solid phase,[5−7] and in aqueous solution.[8] Regarding the theoretical studies of vibrational modes, in addition to the pioneering work of Susi and Ard[6] based on an empirical force field, quantum chemical methods at the SCF level with STO-3G,[7] 6-31G*,[4,8] and 6-31G**[3] basis sets have been used in order to assign the vibrational wavenumbers observed in IR and Raman spectra. Recently correlation effects have also been taken into consideration by performing calculations at the SCF+MP2 level (with a 6-31G* basis set) for evaluating resonance Raman (RR)[8] and NIS[9] intensities of thymine.

In this paper we report new MP2 calculations carried out with extended bases (6-31G and D95V) containing polarization functions. To interpret the NIS (in solid phase) and Raman and IR spectra (in solid as well as aqueous phases) obtained from thymine and its N-deuterated species, we have resorted to scaled quantum mechanical (SQM) calculations.

Experimental Section

Sample Preparation. Thymine (T) (Figure 1) was purchased from Sigma-Aldrich and used as supplied. The N1,N3-deuterated thymine (T-d_2) powder has been obtained from T by repeated cycles of dissolution and stirring in D_2O (Goss Scientific, 99.9%) at 60 °C, recrystallization at room temperature and drying by vacuum evaporation of D_2O. Aqueous solutions of thymine have been prepared at saturation, i.e., ca 2×10^{-2} M. The T-d_2 solution was obtained by dissolving the polycrystalline powder in D_2O.

Experimental Spectra. NIS spectra were obtained on the time-focused crystal analyzer spectrometer TFXA[10,11] located at ISIS pulsed neutron source of the Rutherford Appleton Laboratory (RAL), United Kingdom. Temperature of the experiments has been set sufficiently low ($T = 15$ K) in order to sharpen the vibrational fundamental bands and to decrease the Debye−Waller factor[12] and the intensity of phonon wings (combination bands between the fundamental and lattice modes). Figures 2A and 3A show the NIS spectra of T and T-d_2 species, respectively, in the spectral region below 1850 cm^{-1}.

The whole experimental setup, the data acquisition system, and data treatment for Raman and IR spectra have been described in our recent paper on uracil.[1] NIS spectra have been compared with those provided by IR absorption (Figures 2B and 3B) and Raman scattering ($\lambda_{exc} = 514.5$ nm, Figures 2C and 3C) recorded at low temperature ($T = 15$ K). The temperature dependence of the Raman spectra ($\lambda_{exc} = 514.5$ nm) in the low-wavenumber region is displayed in Figures 2C′ and 3C′. FT Raman spectra ($\lambda_{exc} = 1.06$ μm) of solid samples at room temperature are also reported in Figures 2D and 3D.

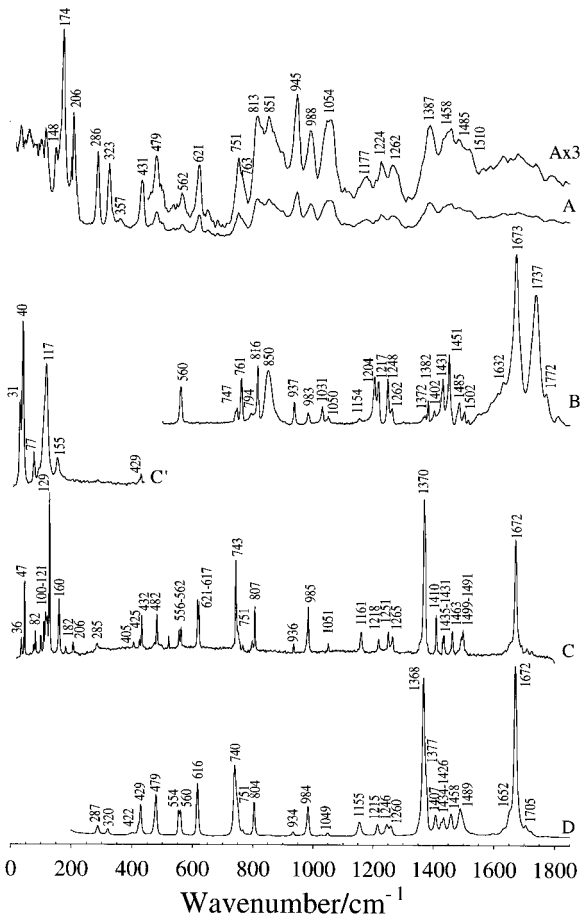

Figure 2. Vibrational spectra of polycrystalline samples of thymine in the region below 1850 cm^{-1}. (A) NIS spectrum at $T = 15$ K; for the sake of clarity the spectral intensity is multiplied by 3 in the region above 450 cm^{-1}. (B) IR spectrum at $T = 15$ K. (C) Raman spectrum ($\lambda_{exc} = 514.5$ nm) at $T = 15$ K. (C′) Low-wavenumber Raman spectrum ($\lambda_{exc} = 514.5$ nm) at room temperature. (D) FT Raman spectrum ($\lambda_{exc} = 1.06$ μm) at room temperature. See Table 1.

To evidence the effects of environment on the vibrational modes, the FT Raman ($\lambda_{exc} = 1.06$ μm) and FT-IR spectra of aqueous solutions of T and T-d_2 species, are shown in the spectral region below 1900 cm^{-1} (Figure 4).

The strong absorption of water, due to the angular deformation mode around 1600 cm^{-1} (δOH) and 1200 cm^{-1} (δOD) in the IR spectra (Figures 4F,H), makes the subtraction of the solvent critical in these spectral regions. Moreover, the water molecules bound to thymine may have δOH (or δOD) band profiles different from those of pure water. So, the contributions of such absorptions are unknown and cannot be correctly eliminated by subtraction of the pure water spectrum and the resulting bands in these spectral regions are thus uncertain.

The whole set of observed vibrational wavenumbers are gathered in Tables 1 and 2 for T and T-d_2, respectively. The report of the solid-phase FT Raman wavenumbers in Tables 1 and 2 is avoided, because they are very close to those observed by excitation at 514.5 nm.

Theoretical Section

Calculation Methods. To estimate structural parameters and harmonic fundamental vibrations of thymine in a state corresponding to that of the gas phase, ab initio quantum mechanical

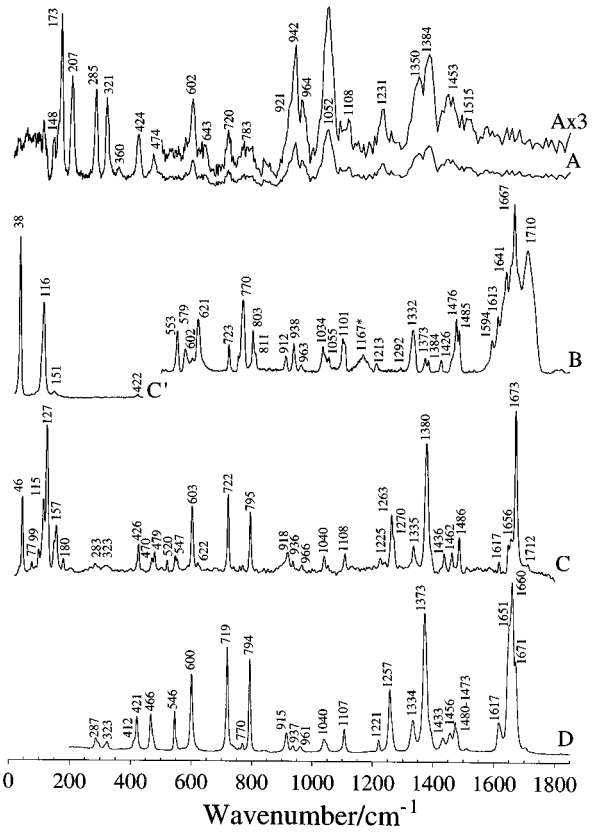

Figure 3. Vibrational spectra of polycrystalline samples of N-deuterated thymine (T-d_2 species) in the region below 1850 cm^{-1}. See the caption of Figure 2 and Table 2.

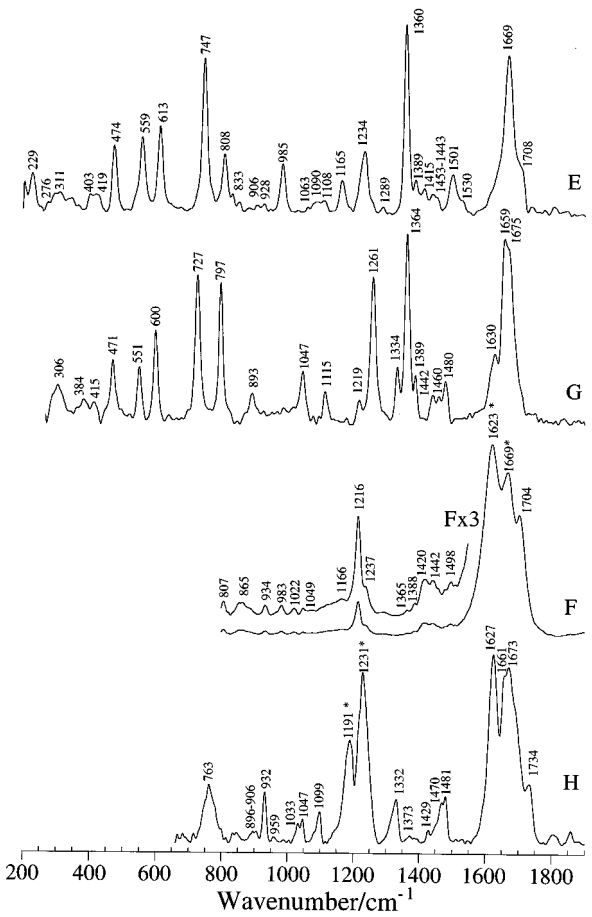

Figure 4. Vibrational spectra of aqueous solutions at room temperature in the spectral region below 1900 cm^{-1}. E and G: FT Raman spectra ($\lambda_{exc} = 1.06\ \mu$m) of T and T-$d_2$ species, respectively. F and H: FT IR spectra of T and T-d_2 species, respectively. See also Tables 1 and 2. The bands marked *, resulting from the subtraction of the water absorption band from the solution spectra, are not reliable (see text).

calculations have been performed at the level of correlation normally used for molecules of medium size: self-consistent field (SCF) plus second-order Møller−Plesset perturbation treatment (MP2). Anharmonic contributions to the force field, i.e., third and higher energy derivatives with respect to atomic coordinates, have not been explicitly evaluated.

All computations were carried out by a GAUSSIAN92 package on a Cray C98 supercomputer platform.[13,14] As in the case of uracil,[1] Gaussian basis functions of double-ζ form (6-31G and D95V basis sets) describing the valence shells of each of the first-row atoms and hydrogens have been selected first. They have been enlarged by adding a nonstandard set of d-polarization functions with exponents equal to 0.75, 0.80, and 0.85 for carbon, nitrogen, and oxygen, respectively. Hereafter, these special basis functions are referred to as 6-31G$^{(*)}$ and D95V$^{(*)}$. However, to further discuss the hydrogen vibrational dynamics, responsible for intense NIS bands, we have undertaken additional calculations with standard basis functions 6-31G** and D95V** (involving p-polarization functions of hydrogen atoms).

Postprocessing of the vibrational modes (redundancy treatment, PED matrix calculation for assigning the normal modes), has been made on the basis of the Wilson GF-method[15] by using a homemade program (BORNS). Details concerning these calculations are found in our previous paper devoted to uracil.[1]

Geometry Optimization and Methyl Group Conformation. Disregarding the hydrogen atoms of the methyl group, thymine has a planar geometry. The orientation of the methyl group corresponding to the molecular energy minima has been discussed in a previous ab initio Hartree−Fock calculation with split-valence 4-21G basis sets.[16] This orientation is the same as that found with more sophisticated calculations, i.e., HF/6-31G* or MP2/6-31G*, carried out recently by Rush and Peticolas.[8]

On the basis of the present calculations and whatever the wave function basis is, four privileged conformations of the CH_3 group with respect to the uracil ring can be obtained by rotations of 30° around the C5−C(H3) axis. Two of these particular conformations have C_s symmetry with one of the methyl hydrogen atoms lying in the ring plane and oriented toward C6 or C4 atoms and the other two symmetrically placed with respect to the heterocyclic ring plane (noted as T_a and T_b conformations, Figure 1). The other two privileged conformations have C_1 symmetry, involving three hydrogen atoms noncoplanar with the ring, one below and the other two above (or vice versa) the molecular ring plane (noted as T_c and T_d conformations in Figure 1). The energy values corresponding to these four privileged conformations as obtained by MP2/6-31G$^{(*)}$ calculations are reported in ref 9. In fact, the conformation T_a corresponds to the minimum of the potential energy curve, while T_b corresponds to a transition state. Finally, both T_c and T_d represent similar intermediate conformations (with the same calculated energy).

Table 3 shows for the T_a conformation the calculated geometrical parameters and the corresponding energies obtained by various MP2 calculations. The experimental geometrical parameters determined from the X-ray diffraction patterns of thymine monohydrate[17] and thymine anhydrate[18] have also been reported in Table 3 for comparison.

Choice of Symmetrical Internal Coordinates. All of the vibrational mode calculations have been performed with the geometrical parameters related to the T_a conformation (Table

TABLE 1: Comparison between Experimental and Scaled 6-31G* Wavenumbers (in cm^{-1}) for Thymine in the Spectral Region below 1800 cm^{-1} [a]

experimental						
NIS	Raman		IR			
A	C	E	B	F	calcd	potential energy distribution (%)
			A′ Species			
			1772 (w)			
		1708 (sh)	1737 (s)	1704 (s)	1760	C2═O2 (56); C2−N3 (7)
	1672 (vs)	1669 (s)	1673 (vs)		1728	C5═C6 (28); C4═O4 (25); C4−C5 (10)
	1652 (sh)		1632 (w)		1679	C4═O4 (41); C5═C6 (13); N1C6H (9); C5═C6H (7); C6−N1 (5)
1510 (sh)		1530 (sh)			1524	C2═O2 (13); C4−C5 (12); C6N1H (11), C4═O4 (10); C6−N1 (9), N3−C4 (7); C2N1H (7); C5−C(H3) (5)
	1499 (m)	1501 (m)	1502 (vw)	1498 (w)	1493	CH_3-antisym bend. 1 (44); CH_3-antisym bend. 2 (15); CH_3-antisym rock. 2 (9); C6N1H (7)
1485 (m)						
	1491 (m)		1485 (m)		1472	CH_3-antisym bend. 1 (17); C2N1H (15); C6N1H (11); C4−C5 (10); CH_3-antisym bend 2 (6)
	1435 (m)	1443 (w)	1431 (m)	1442 (m)	1428	N1C6H (17); C5═C6H (14); C5═C6 (14); CH_3-antisym bend. 1 (13); N1−C2 (7)
	1431 (m)					
	1410 (m)	1415 (w)	1402 (w)	1420 (m)	1406	C4N3H (26); C2N3H (24); C2═O2 (16); C4═O4 (15)
1387 (m)	1370 (vs)	1389 (m)	1382 (w)	1388 (w)		
		1360 (vs)	1372 (w)	1365 (vw)	1373	CH_3-sym bend. (36); CH_3-sym rock. (35); C5−C(H3) (17)
1262 (m)	1265 (w)	1289 (w)	1262 (w)		1270	C2−N3 (23); N1−C2 (15); C5−C(H3) (12); C4−C5 (10); N1C6H (8)
	1251 (w)		1248 (s)			
1224 (m)	1218 (w)	1234 (s)	1217 (m)	1237 (sh)	1220	C6−N1 (42); C5−C(H3) (19); C6N1H (10)
			1204 (s)	1216 (s)		
1177 (m)	1161 (w)	1165 (m)	1154 (vw)	1166 (vw)	1174	N3−C4 (35); C6−N1 (9); C5C(H3) (9); CH_3-antisym rock. 2 (8)
1054 (m)		1063 (w)	1031 (w)	1022 (w)	1028	CH_3-antisym rock. 2 (60)
988 (m)	985 (m)	985 (m)	983 (m)	983 (w)	973	CH_3-antisym rock. 2 (21); N1−C2 (20); C2−N3 (10); C4−C5 (9)
	807 (m)	808 (m)	794 (vw)	807 (vw)	804	C5−C(H3) (25); N1−C2 (11); N1C2N3 (8); C6N1C2 (8); C2═O2 (8); N1C6C5 (7)
751 (m)	743 (s)	747 (s)			755	C4−C5 (29); C5−C(H3) (20); N1−C2 (7); C5═C6 (7)
621 (m)	621 (m)	613 (m)			610	C5C4═O4 (21); N1C2═O2 (14); N3C2═O2 (13); N3C4═O4 (8); C4C5C(H3) (7)
	617 (m)					
562 (w)	562 (w)	559 (m)	560 (m)		545	C2N3C4 (14); N3C4═O4 (11); N1C6C5 (10); C2−N3 (10); N3C4C5 (9); N3C4 (8); N1C2═O2 (7)
	556 (w)					
479 (w)	482 (m)	474 (m)			460	C4C5═C6 (16); N3C2═O2 (12); N1C2N3 (11); C5−C(H3) (9); N3C4C5 (9); C6N1C2 (8); N3−C4 (6); N3C4═O4 (6)
357 (w)	405 (vw)	403 (w)			389	N1C2═O2 (20); N3C2═O2 (14); N3C4═O4 (12); C5C4═O4 (12); N3−C4 (9); C2−N3 (7); C2N3C4 (6)
286 (s)	285 (vw)	276 (vw)			281	C4C5C(H3) (36); C6═C5C(H3) (32); C5C4═O4 (8); CH_3-antisym rock. 2 (7)
			A″ Species			
1458 (s)	1463 (m)	1453 (m)	1451 (s)		1461	CH_3-antisym bend. 2 (69); CH_3-antisym bend. 1 (23); CH_3-antisym rock. 1 (8)
1054 (m)	1051 (w)	1108 (w)	1050(vw)	1049(vw)	1071	CH_3-antisym rock. 1 (85)
		1090 (w)				
945 (m)	936 (w)	928 (w)	937 (m)	934 (w)	945	ω(C6H) (52); τ(N1C6) (18); τ(C5═C6) (14); ω(C4═O4) (6)
851 (w)		833 (sh)	850 (m)	865 (w)	849	ω(N3H) (35); τ(N3C4) (17); τ(N3C2) (15); ω(C6H) (14); ω(N1H) (6)
813 (m)			816 (s)		815	ω(N1H) (21); ω(C6H) (18); τ(N1C2) (16); ω(N3H) (12); τ(N3C2) (13); τ(N1C6) (9); τ(N3C2) (9); τ(N3C4) (8)
763 (sh)	751 (sh)		761 (m)		755	ω(C2═O2) (84); ω(C4═O4) (7)
751 (m)			747 (w)		743	ω(C4═O4) (54); ω(C6H) (20); ω(C2═O2) (8); C5−C(H3) wag (9)
431 (s)	432 (m)	419 (w)			431	C5−C(H3) wag (29); ω(C6H) (29); ω(N1H) (17); ω(C4═O4) (6)
	425 (w)					
323 (s)	320 (vw)	311 (w)			319	C5−C(H3) wag (43); ω(N3H) (10); CH_3-antisym rock. 1 (9); ω(C6H) (7); ω(C4═O4) (7)
206 (s)	206 (w)	229 (m)			210	ω(N3H) (42); C5−C(H3) wag (15); ω(N1H) (11); τ[C5C(H3)] (9); τ(C4C5) (7)
174 (vs)	182 (vw)				173	τ[C5C(H3)] (76); C5C(H3) wag (7)
148 (m)	160 (m)				143	ω(N1H) (36); ω(N3H) (18); τ(N3C2) (15); τ(N1C2) (12); ω(C4═O4) (10)

[a] Assignments are based on the internal coordinates for which the potential energy distribution (PED) is reported in percent (only contributions greater than 6%). See also Figures 2 and 4 and Figures 8 and 9. The scaled wavenumbers above 1800 cm^{-1} are 2932 (CH_3-sym str), 2993 (CH_3-antisym str 1), 3001 (CH_3-antisym str 2), 3065 (C6H), 3434 (N3H), 3477 (N1H). (A) NIS spectrum at 15 K. (B) IR spectrum in solid phase at 15 K. (C) Raman spectra in solid phase at 15 K, λ_{exc} = 514.5 nm and (E) FT Raman spectrum (λ_{exc} = 1.06 μm) of aqueous solution at room temperature. (F) FT IR spectrum of aqueous solution at room temperature. vs: very strong, s: strong, m: medium, w: weak, vw: very weak, sh: shoulder, br: broad.

3). The symmetrical coordinates reflecting the local symmetry (C_{3v}) of the methyl group, belonging to A_1 and E irreducible representations, have been used in our normal-mode calculations (Table 4). The lowering of the methyl group symmetry from C_{3v} to C_s (when it is connected to the uracil ring), allows the A_1 symmetrical coordinates to appear in the PED of the A′ normal modes. The doubly degenerate antisymmetrical coordinates (E species) appear among both the A′ and A″ normal

TABLE 2: Comparison between Experimental and Scaled 6-31G* Wavenumbers (in cm^{-1}) for T-d2 Species in the Spectral Region below 1800 cm^{-1} [a]

experimental						
NIS	Raman		IR			
A	C	G	B	H	calcd	potential energy distribution (%)
						A′ Species
	1712 (vw)	1675 (sh)	1710 (s)	1673 (vs)	1735	C2═O2 (66); C2−N3 (7); N1−C2 (6)
	1673 (vs)	1659 (vs	1667 (vs)	1661 (sh)	1718	C5═C6 (31); C4═O4 (24); C4−C5 (9); N1C6H (8)
	1656 (w)	1630 (m)	1641 (m)	1627 (vs)	1666	C4═O4 (49); C4−C5 (11); C5═C6 (10); N1C6H (8); C5═C6H (6)
	1617 (w)		1613 (w)			
			1594 (w)			
1515 (m)					1511	C4−C5 (16); C4═O4 (16); N3−C4 (10); CH_3-antisym bend 1 (10); CH_3-antisym rock. 2 (7)
	1486 (m)	1480 (m)	1485 (m)	1481 (s)	1484	CH_3-antisym bend 1 (51); CH_3-antisym bend 2 (17); CH_3-antisym rock. 2 (5)
	1436 (w)	1442 (m)	1426 (w)	1429 (m)	1427	N1C6H (22); C5═C6H (16); C5═C6 (15); CH_3-antisym bend 1 (14); N1−C2 (7); C5−C(H3) (6)
1384 (m)	1380 (vs)	1389 (m)	1384 (w)	1373 (w)	1373	CH_3-sym bend (37); CH_3-sym rock. (35); C5−C(H3) (18);
		1364 (vs)	1373 (w)			
1350 (m)	1335 (w)	1334 (m)	1332 (m)	1332 (m)	1353	C6−N1 (29); C2−N3 (18); C2═O2 (10); C2N1D (10); C6N1D (7)
	1270 (sh)	1261 (s)	1292 (vw)		1269	C2−N3 (22); N1−C2 (15); C6−N1 (13); N3−C4 (12); C5−C(H3) (8); C4−C5 (8)
	1263 (m)					
1231 (m)	1225 (w)	1219 (w)	1213 (vw)		1241	N3−C4 (21); C5−C(H3) (19); C2N3D (14); C4N3D (8); C2═O2 (8)
1108 (w)	1108 (w)	1115 (m)	1101 (m)	1099 (m)	1120	C5−C(H3) (15); C4N3D (12); N1−C2 (11); N3−C4 (11); C2N3D (8); N3C4═O4 (7)
	1040 (w)	1047 (m)	1034 (m)	1033 (w)	1062	CH_3-antisym rock. 2 (56); C6N1D (11); C2N1D (7)
964 (m)	966 (w)		963 (w)	959 (vw)	962	CH_3-antisym rock. 2 (27); C2N1D (22); C6N1D (18); C6−N1 (11)
921 (sh)	918 (m)	893 (w)	912 (w)	906 (w)	879	C2N3D (18); N1−C2 (10); C2−N3 (10); C4N3D (9); C6N1C2 (8)
				896 (w)		
783 (br, m)			811 (sh)		783	N1−C2 (24); C2−N3 (10); C5−C(H3) (7); N1C6═C5 (7); C4C5═C6 (6)
720 (w)	722 (s)	727 (s)	723 (w)		730	C4−C5 (24); C5−C(H3) (26); C4N3D (9); C5═C6 (7); N1C2N3 (7)
	603 (s)	600 (s)	602 (vw)		592	C5C4═O4 (20); N3C2═O2 (12); N1C2═O2 (11); C4C5C(H3) (7); C5═C6 (6)
			579 (w)			
	547 (m)	551 (m)	553 (m)		534	N3C4═O4 (13); C2N3C4 (12); N1C6═C5 (10); C2−N3 (9); N3−C4 (9); N1C2═O2 (8); C2N3D (7); N3C4C5 (6)
	520 (w)					
474 (m)	479 (w)	471 (m)			456	C4C5═C6 (15); N3C2═O2 (12); N1C2N3 (11); N3C4C5 (10); C5−C(H3) (8); C6N1C2 (8); N3C4═O4 (8)
	470 (sh)					
360 (w)		384 (w)			387	N1C2═O2 (21); N3C2═O2 (14); C5C4═O4 (12); N3C4═O4 (11); N3−C4 (9); C2−N3 (7); C2N3C4 (7)
285 (s)	283 (w)				281	C4C5C(H3) (36); C6═C5C(H3) (32); C5C4═O4 (8); CH_3-antisym rock. 2 (7)
						A″ Species
1453 (w)	1462 (w)	1460 (m)	1476 (s)	1470 (s)	1461	CH_3-antisym bend 2 (69); CH_3-antisym bend 1 (23); CH_3-antisym rock. 1 (8)
1052 (s)			1055 (w)	1047 (w)	1070	CH_3-antisym rock. 1 (86)
942 (s)	936 (w)		938 (m)	932 (s)	930	ω(C6H) (62); τ(C5═C6) (16); τ(N1C6) (10); ω(C4═O4) (7)
783 (br, m)	795 (s)	797 (s)	803 (m)	763 (s)	755	ω(C2═O2) (84); ω(C4═O4) (7)
			770 (s)		743	ω(C4═O4) (54); ω(C6H) (20); C5−C(H3) wag (10); ω(C2═O2) (8)
643 (m)	622 (w)		621 (m)		630	τ(N1C6) (20); ω(N3D) (17); τ(N1C2) (15); ω(N1D) (14); ω(C6H) (11); τ(N3C4) (9); τ(N3C2) (6)
602 (m)		600 (m)			599	ω(N3D) (36); τ(N3C2) (17); τ(N3C4) (16); ω(N1D) (11); τ(N1C2) (9); τ(N1C6) (8)
424 (s)	426 (m)	415 (w)			421	ω(C6H) (28); C5−C(H3) wag (26); ω(N1D) (23); τ(C5═C6) (8); ω(C4═O4) (6)
321 (s)	323 (w)	306 (m)			318	C5−C(H3) wag (44); ω(N3D) (9); ω(C4═O4) (8); ω(C6H) (6)
207 (s)					210	ω(N3D) (42); C5−C(H3) wag (15); ω(N1D) (10); τ[C5−C(H3)] (9); τ(C4C5) (7)
173 (vs)	180 (w)				172	τ[C5−C(H3)] (75); C5−C(H3) wag (8)
148 (m)	157 (m)				143	ω(N1D) (36); ω(N3D) (18); τ(N3C2) (15); τ(N1C2) (12); ω(C4═O4) (10)

[a] The scaled wavenumbers above 1800 cm^{-1} are 2519 (N3D), 2552 (N1D) 2932 (CH_3-sym str), 2993 (CH_3-antisym str 1), 3003 (CH_3-antisym str 2), 3065 (C6H). (G) FT Raman spectrum ($\lambda_{exc} = 1.06$ μm) of aqueous solution at room temperature. (H) FT IR spectrum of aqueous solution at room temperature. See also the caption of Table 1 and Figures 3 and 4.

mode assignments, except for the antisymmetrical rocking modes which are transformed to either the A′ or the A″ species (Tables 1 and 2).

Scaling of the ab Initio Force Field. To improve the agreement between the calculated wavenumbers and those observed in the solid state and aqueous phase, as well as to get a good fit with the NIS intensities in solid phase, the molecular force field of thymine has been scaled. The scaling procedure of the ab initio force field has been fully described in our previous paper on uracil.[1] Briefly, force constants related to bond stretchings and angular bendings of the uracil ring as well as those related to the methyl group vibrational motions have been scaled by using the Pulay method.[19,20] Table 4 gives the values of the 24 scaling factors used in the vibrational mode calculations of both T and T-d_2 species. They have been compared with those previously used in uracil,[1] for scaling the

TABLE 3: Thymine Geometry Parameters As Obtained by Various MP2 Calculations[a]

			calculated			
	exptl[b]	exptl[c]	MP2/6-31G(*)	MP2/6-31G**	MP2/D95V(*)	MP2/D95V**
			Bond Lengths/Å			
N1−C2	1.355	1.314	1.386	1.385	1.387	1.387
C2−N3	1.361	1.345	1.386	1.386	1.388	1.388
N3−C4	1.391	1.413	1.403	1.402	1.405	1.405
C4−C5	1.447	1.476	1.463	1.462	1.468	1.468
C5═C6	1.349	1.369	1.355	1.354	1.362	1.362
C6−N1	1.382	1.408	1.380	1.379	1.384	1.383
N1−H	0.79		1.013	1.008	1.016	1.010
C2═O2	1.234	1.246	1.225	1.225	1.230	1.229
N3−H	0.81		1.017	1.012	1.020	1.015
C4═O4	1.231	1.193	1.230	1.230	1.235	1.234
C5−C(H3)	1.503	1.522	1.497	1.495	1.502	1.500
C(H3)−H	0.97		1.094	1.089	1.097	1.092
	0.88					
	0.80					
C6−H	0.86		1.087	1.088	1.088	1.084
			Bond Angles/deg			
C2−N1−H	112.0		114.939	114.923	114.981	115.140
C6−N1−C2	122.8	123.0	124.052	124.087	123.876	123.872
C6−N1−H	125.0		121.010	120.989	121.143	120.989
N1−C2═O2	122.7	122.0	123.552	123.564	123.461	123.487
N1−C2−N3	115.2	118.0	112.224	112.216	112.613	112.564
N3−C2═O2	122.1	121.0	124.224	124.220	123.926	123.949
C2−N3−H	108.0		115.429	115.366	115.358	115.354
C2−N3−C4	126.3	126.0	128.616	128.609	128.415	128.477
C4−N3−H	125.0		115.955	116.024	116.227	116.168
N3−C4═O4	118.3	121.0	120.703	120.750	120.472	120.538
N3−C4−C5	115.6	114.0	114.354	114.322	114.513	114.446
C5−C4═O4	126.1	125.0	124.943	124.929	125.015	125.017
C4−C5−C(H3)	119.0	119.0	117.654	117.682	118.002	118.088
C4−C5═C6	118.2	119.0	118.359	118.427	118.182	118.184
C6═C5−C(H3)	122.8	122.0	123.987	123.891	123.816	123.729
N1−C6−H	111.0		115.227	115.275	115.404	115.395
N1−C6−C5	121.8	120.0	122.396	122.339	122.401	122.457
C5═C6−H	127.0		122.377	122.385	122.194	122.148
C5−C(H3)−H′	126.0		111.046	110.993	110.786	110.723
C5−C(H3)−H″	123.0		110.548	110.509	110.338	110.372
C5−C(H3)−H‴	118.0		110.548	110.509	110.338	110.372
H′−C(H3)−H″	96.0		108.817	108.832	109.021	109.009
H′−C(H3)−H‴	96.0		108.817	108.832	109.021	109.009
H″−C(H3)−H‴	89.0		106.951	107.060	107.253	107.275
methyl group torsions/deg						
C6−C5−C(H3)−H′			0.0	0.0	0.0	0.0
C6−C5−C(H3)−H″			120.884	120.842	120.829	120.794
C6−C5−C(H3)−H‴			−120.884	−120.842	−120.829	−120.794
total energy/au			−452.815 222	−452.861 042	−452.868 189	−452.922 287
Z.P.V./au			0.1166	0.1172	0.1160	0.1368

[a] The experimental results are taken from the X-ray diffraction patterns of (*b*) thymine monohydrate[17] and (*c*) thymine anhydrate.[18]

in-plane vibrational modes. Deviations from the uracil scaling factors do not exceed 24%: the maximum deviation concerns the C−C bond stretch scaling (due to the presence of a CH_3 group). This confirms the idea of transferring the scaling factors from one molecule to a structurally similar one, of course when the geometry optimization and force field calculations have been performed at the same level of theory. The majority of scaling factors lie between 0.8 and 1.1, i.e., close to unity. The only exception is the large value (1.40) selected as the scaling factor for the methyl torsion coordinate. This value made possible the wavenumber upshift of the methyl torsion mode calculated at 149 cm^{-1} (with unscaled force field) to 173 cm^{-1} (with scaled force field). The other force constants related to the ring torsional and wagging motions have been scaled separately by using the previously reported method:[1] the diagonal force constants have been left unchanged with respect to the primitive theoretical values, and only the off-diagonal terms, reflecting the interactions between the out-of-plane internal coordinates, have been modified by the least-squares technique in order to improve both vibrational wavenumbers and NIS intensities.

Discussion

Wavenumbers from spectra recorded in different phases (gas, solution and solid) have been taken as reference in testing the validity of the nonscaled and scaled ab initio force fields. Moreover, the estimation of NIS intensities requires both the vibrational wavenumbers and normalized atomic displacements, especially those corresponding to the hydrogen atoms. For this reason, the simulation of NIS spectra can be considered as an additional proof for checking the reliability of our theoretical force fields, the extension of the used basis sets and the empirical scaling. As previously shown in guanine,[21] adenine,[22] and uracil,[1,9] the internal modes (molecular modes) and external modes (lattice modes) are observed in two distinct spectral regions in NIS spectra. This simplifies considerably the treatment of the internal modes and the analysis of their coupling

TABLE 4: Scaling Factors for Thymine[a]

coordinate specification	uracil	thymine
ν(C−N)	0.942	0.903
ν(C−C)	0.952	1.180
ν(C═C)	0.834	0.890
ν(C═O)	0.792	0.831
ν(C−H)	0.897	0.889
ν(N−H)	0.905	0.905
δ(C−N−H)	1.032	1.058
δ(N−C−H)	1.069	1.198
δ(N−C−C)	0.993	0.933
δ(C−N−C)	0.996	0.996
δ(N−C−N)	0.992	0.992
δ(C−C═C)	1.144	1.032
δ(N−C═C)	1.144	1.043
δ(N−C═O), δ(C−C═O)	1.092	1.048
δ(C−C−H), δ(C═C−H)	0.992	1.058

coordinate specification (methyl group)	thymine
ν[C5−C(H3)]	0.957
δ[C−C−C(H3)]	1.012
CH_3-sym str = $(1/\sqrt{3})[\nu(CH')+\nu(CH'')+\nu(CH''')]$	0.892
CH_3-antisym str 1 = $(1/\sqrt{2})[\nu(CH'')-\nu(CH''')]$	0.880
CH_3-antisym str 2 = $(1/\sqrt{6})[2\nu(CH')-\nu(CH'')-\nu(CH''')]$	
CH_3-sym bend = $(1/\sqrt{3})[\delta(H'CH'')+\delta(H'CH''')+\delta(H''CH''')]$	0.810
CH_3-antisym bend 1 = $(1/\sqrt{2})[\delta(H'CH''')-\delta(H''CH''')]$	0.910
CH_3-antisym bend 2 = $(1/\sqrt{6})[2\delta(H'CH'')-\delta(H'CH''')-\delta(H''CH''')]$	
CH_3-sym rock = $(1/\sqrt{3})[\delta(C5CH')+\delta(C5CH'')+\delta(C5CH''')]$	0.932
CH_3-antisym rock 1 = $(1/\sqrt{2})[\delta(C5CH'')-\delta(C5CH''')]$	0.954
CH_3-antisym rock 2 = $(1/\sqrt{6})[2\delta(C5CH')-\delta(C5CH'')-\delta(C5CH''')]$	
τ[C5−C(H3)]	1.400

[a] The values of the similar scaling factors found in uracil[1] are reported for comparison.

with the external ones. In thymine (Figures 2 and 3), lattice modes give rise to bands below 140 cm^{-1}.

Experimental Spectra in the Gas Phase: Wavenumbers and NIS Intensities Calculated with a Nonscaled Force Field. The theoretical vibrational wavenumbers of thymine calculated with a nonscaled force field are compared with those obtained experimentally for the gas phase.[2] As in the case of uracil[1] acceptable values of the ν_{exp}/ν_{calc} ratios are found (located in the 0.922−1.244 range), whatever are the basis functions used in these calculations (Table 5).

In Figure 5 are shown the first-order simulated NIS spectra obtained with different nonscaled force fields derived by different MP2 calculations. The main striking effects revealing the disagreement between the experimental and simulated NIS spectra can be mentioned as follows: (i) the NIS simulated intensity is largely overestimated around 695 and 560 cm^{-1}. Table 5 shows that these calculated modes correspond to the out-of-plane vibrational motions involving the N3 and N1 atoms, respectively, which are both hydrogen bonded in thymine crystalline lattices.[17,18] (ii) As far as the methyl group motions are concerned, one should emphasize the overestimation of the simulated NIS band around 1530 cm^{-1} which mainly arises from CH_3 bending motions (Figure 5). Likewise, the intensity of the methyl torsional mode (calculated around 150 cm^{-1}) is also overestimated. These calculated intensities are not improved even when p-orbitals on hydrogen atoms (6-31G** basis functions) are added. Moreover, the most advanced bases used in this work (6-31G** and D95V**) lead generally to the shortening of the C−H and N−H bond lengths (Table 3) and consequently to an increase of the corresponding stretching wavenumbers which are already too high (Table 5).

We conclude that the disagreement between the experimental and simulated NIS spectra with nonscaled force fields is independent of the basis functions used here and can only be improved by an adequate scaling procedure (see next section).

Experimental Spectra in the Condensed Phase: Wavenumbers and NIS Intensities Calculated with a Scaled Force Field. As in the case of uracil,[1] the starting point in the scaling procedure was the calculated force field obtained with 6-31G(*) basis sets. The vibrational wavenumbers obtained by scaled force field are reported in the Tables 1 and 2 for T and T-d_2 species, respectively. In Figures 6 and 7, we report NIS simulated spectra calculated for these two isotopic species, involving the first-order spectra as well as the combinations between the lattice and fundamental modes (up to the third order).[1] To give a picture of each normal mode harmonic dynamics, graphical representations of the A′ and A″ modes located below 2000 cm^{-1} are shown in Figures 8 and 9, respectively.

In the following discussion, we overview the most characteristic vibrational features, reminding the changes occurring in the NIS, IR, and Raman spectra from uracil to thymine. The intense NIS bands involving mainly the vibrational motions of the methyl hydrogen atoms, will guide us to attain this goal.

The 1750−1600 cm^{-1} spectral region involves mainly the C═O and C═C bond-stretching motions. As for uracil, NIS spectra give rise to a broad and weak band (Figure 2) centered around 1600 cm^{-1} which is canceled for the T-d_2 species (Figure 3). This effect should be correlated to the coupling of δNH with carbonyl stretching motions, which is not reproduced by the present calculations. Optical spectra in this region reveal more intense and resolved bands, allowing their assigments by the theoretical wavenumbers to be performed (Tables 1 and 2). The optical spectra in solid phase are more structured than those recorded in solution. As Figures 2−4 show, the shifts of the C═O and C═C stretch wavenumbers from the solid phase to solution, exhibit the effect of environment on these vibrational modes. The two carbonyls which are known to be involved in intermolecular H-bonds in the crystal lattice,[17,18] should be more weakly H-bonded to water in solution.

TABLE 5: Comparison Between Nonscaled Calculated Wavenumbers and Experimental Data (Gas Phase, Ref 2)[a]

exptl (gas)		calculated				
Raman	IR	6-31G(*)	6-31G**	assignment	D95V(*)	assignment
				A′ Species		
3434	3430	3654 *(0.939)*	3728 *(0.920)*	N1−H	3647 *(0.940)*	N1−H
3407	3402	3610 *(0.942)*	3682 *(0.924)*	N3−H	3602 *(0.944)*	N3−H
3020	3021	3250 *(0.930)*	3288 *(0.919)*	C6−H	3243 *(0.932)*	C6−H
2970	2966	3201 *(0.927)*	3240 *(0.915)*	CH_3-antisym str 2.	3191 *(0.929)*	CH_3-antisym str 2.
2931	2938	3104 *(0.947)*	3136 *(0.937)*	CH_3-sym str	3080 *(0.954)*	CH_3-sym str
1722	1720	1866 *(0.922)*	1867 *(0.921)*	C2═O	1840 *(0.935)*	C2═O
1714	1710	1805 *(0.947)*	1806 *(0.947)*	C4═O	1781 *(0.947)*	C4═O
1622	1624	1735 *(0.936)*	1739 *(0.934)*	C═C; C4═O	1719 *(0.945)*	C═C; C4═O
1494	1491	1533 *(0.973)*	1536 *(0.971)*	C−N ; CN1H; C4−C5	1526 *(0.977)*	CH_3-antisym bend. 1; C6N1H
1462	1466	1554 *(0.943)*	1555 *(0.943)*	CH_3-antisym bend. 1; CH_3-antisym bend. 2	1540 *(0.952)*	CH_3-antisym bend. 1; CH3- antisym. bend. 2
1425	1421	1458 *(0.975)*	1458 *(0.975)*	CN1H; C2−N3; C4−C5	1450 *(0.980)*	CN1H; C2−N3; C4−C5
1385	1381	1420 *(0.973)*	1419 *(0.973)*	CN3H; C6−H bend	1414 *(0.977)*	CN3H; N3−C4
1378	1374	1471 *(0.934)*	1470 *(0.935)*	CH_3-sym bend; CH_3-sym rock; C5−C(H3)	1462 *(0.940)*	CH_3-sym bend; CH_3-sym rock; C5−C(H3)
1340	1337	1413 *(0.946)*	1415 *(0.945)*	CN3H; C2−N3	1404 *(0.952)*	C6−H bend; N1−C2
1271	1269	1238 *(1.025)*	1235 *(1.027)*	C−N; C5−C(H3)	1232 *(1.030)*	C−N; C5−C(H3)
1209	1208	1284 *(0.941)*	1285 *(0.941)*	C5−C(H3); C6−N1	1283 *(0.942)*	C5−C(H3); C6−N1
1161	1160	1190 *(0.975)*	1190 *(0.975)*	N3−C4; CH_3-antisym rock. 2; C6−N1	1184 *(0.980)*	N3−C4; C6−N1; CH_3-antisym rock. 2
1030	1028	1045 *(0.984)*	1046 *(0.984)*	CH_3-antisym rock. 2	1042 *(0.987)*	CH_3-antisym rock. 2
1016	1018	988 *(1.030)*	988 *(1.030)*	N1−C2; CH_3-antisym rock. 2	986 *(1.032)*	N1−C2; CH_3-antisym rock. 2
947	944	813 *(1.161)*	815 *(1.158)*	C5−C(H3); N1−C2; ring bend	810 *(1.165)*	C5−C(H3); N1−C2; ring bend
746	750	750 *(1.000)*	750 *(1.000)*	C4−C5; C5−C(H3)	746 *(1.005)*	C4−C5; C5−C(H3)
591	592	607 *(0.975)*	607 *(0.975)*	C═O bend	605 *(0.979)*	C═O bend
537	540	546 *(0.989)*	547 *(0.987)*	C2N3C4; N3C4═O; N1C6C5	545 *(0.991)*	C2N3C4; N3C4═O; N1C6C5
481	480	461 *(1.041)*	461 *(1.041)*	C4C5C6; N3C2═O2; N1C2N3	460 *(1.043)*	C4C5C6; N3C2═O2; N1C2N3
384	381	386 *(0.987)*	386 *(0.987)*	NC2═O; NC4═O	386 *(0.987)*	NC2═O; NC4═O
		279	278	CC5−C(H3)	280	CC5−C(H3)
				A″ Species		
2945	2950	3190 *(0.925)*	3228 *(0.914)*	CH_3-antisym str 1	3181 *(0.927)*	CH_3-antisym str 1
1440	1437	1529 *(0.940)*	1528 *(0.940)*	CH_3-antisym bend. 2; CH_3-antisym bend. 1	1510 *(0.952)*	CH_3-antisym bend 2; CH_3-antisym bend. 1
1066	1064	1089 *(0.977)*	1090 *(0.976)*	CH_3-antisym rock. 1	1089 *(0.977)*	CH_3-antisym rock. 1
920	917	880 *(1.042)*	884 *(1.037)*	ω(C6−H); τ(C5═C6)	859 *(1.068)*	ω(C6−H); τ(C5═C6)
808	808	730 *(1.107)*	723 *(1.117)*	ω(C2═O); ω(N3H); ω(C4═O)	747 *(1.082)*	ω(C2═O); ω(C4═O); ω(N3H)
712	710	747 *(0.950)*	742 *(0.942)*	ω(C2═O); ω(C4═O)	756 *(0.939)*	ω(C4═O); ω(C2═O)
658	655	697 *(0.940)*	695 *(0.942)*	ω(C2═O); ω(C4═O); τ(N3C4); τ(N3C2)	691 *(0.948)*	ω(N3H); τ(N3C4); τ(N3C2)
559	560	568 *(0.986)*	572 *(0.979)*	τ(CN); ω(N1H)	553 *(1.013)*	τ(CN); ω(N1H)
465	469	377 *(1.244)*	375 *(1.251)*	C5−C(H3) wag; ω(N1H); τ(C5═C6); ω(C4═O)	388 *(1.209)*	C5−C(H3) wag; ω(N1H); ω(C4═O); τ(C5═C6)
	357	292 *(1.223)*	291 *(1.227)*	C5−C(H3) wag; ω(N1H)	288 *(1.240)*	C5−C(H3) wag; ω(N1H)
	139	149 *(0.933)*	146 *(0.986)*	τ[C5−C(H3)]	152 *(0.914)*	τ[C5−C(H3)]
		143	141	ω(N3H); τ(C4−C5); τ(N3−C4)	147	ω(N3H); τ(C4−C5); τ(N3−C4)
		109	109	ω(N1H); τ(ring)	107	ω(N1H); τ(ring)

[a] The values in brackets are the ν_{exp}/ν_{calc} ratios. For each vibrational mode a limited assignment based on the major internal coordinates is also reported. The numbering of the atoms is avoided when several internal coordinates of the same group are found in the description of the PED.

In the 1550−1300 cm^{-1} spectral region, the NIS and optical spectra of thymine yield additional bands (Figure 2) as compared to those of uracil.[1] The methyl group as well as the ring hydrogen motions take part in the modes observed in this region. One can assign the CH_3 characteristic bending modes by the present calculations.

The presence of the methyl group also perturbs the uracil vibrational modes in the 1300−1100 cm^{-1} spectral region. NIS spectrum of uracil[1] reveals a broad and intense band peaking around 1251 cm^{-1} involving the in-plane N−H angular bending. In thymine, this band is decomposed into three components at 1262, 1224, and 1177 cm^{-1} (Figure 2). According to our calculations, the coupling of the C5−C(H3) bond stretch with the ring bond stretch and angle deformations is responsible for this effect (Table 1). These components splitted by the crystal field are observed with a higher resolution in Raman and IR spectra of the solid phase. Upon deuteration, NIS and optical spectra show that the number of observed bands is reduced in this spectral range. Part of the change in going from T to T-d_2 species is quite reproduced by the calculations. Because of the underestimation of the N−H angular deformation contribution in the calculated mode at 1270 cm^{-1} for T species (Table 1, Figure 8) the experimental isotopic shift in this region cannot be well reproduced (Figure 7). The effect of environment in this range should also be emphasized (comparison between solid-phase and solution optical spectra, Figures 2 and 4).

CH_3-rocking motions, alone or coupled with the ring-stretching motions of thymine, give rise to two intense NIS bands at 1054 and 988 cm^{-1}. The former is observed weakly in optical spectra, whereas the latter appears as a medium Raman band for both solid and aqueous phases.

Below 950 cm^{-1}, wagging and torsional motions give rise to medium and intense bands on NIS spectra. Some of these modes are also observed in IR spectra. In our previous paper on uracil,[1] we have mentioned the particular difficulties related to the calculation of the wavenumbers and NIS intensities of

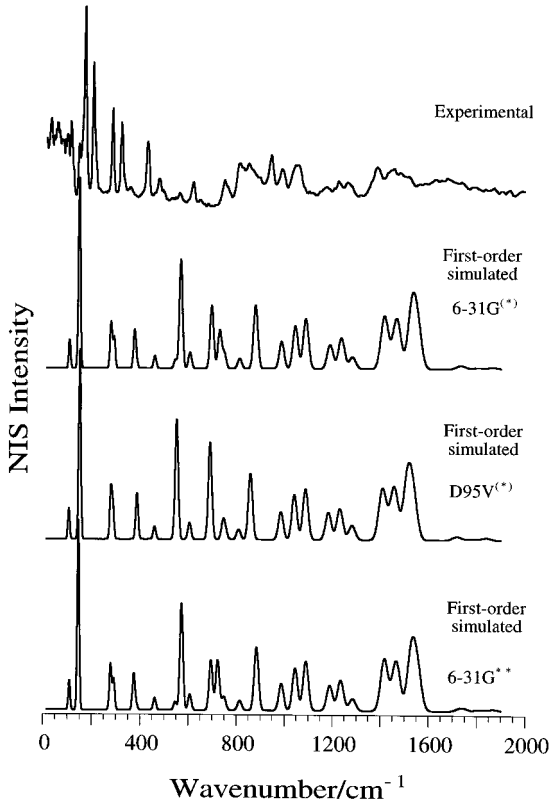

Figure 5. Comparison between experimental and first-order simulated NIS spectra obtained with various nonscaled ab initio force fields in the spectral region below 2000 cm^{-1}.

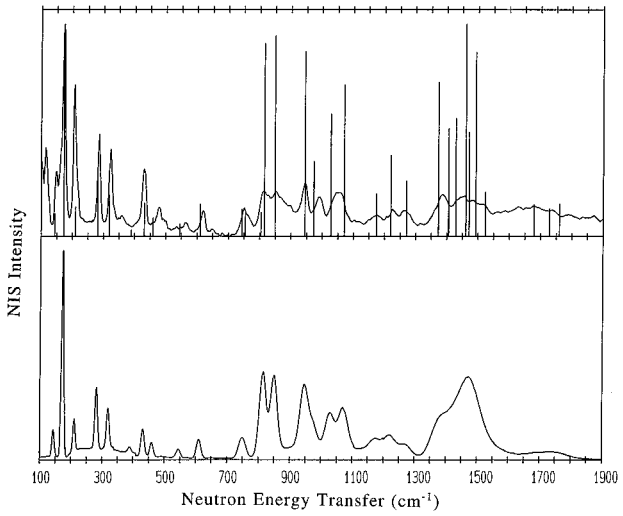

Figure 6. Comparison between experimental (top) and simulated NIS (with scaled 6-31G(*) force field) spectra for thymine in the 100−1900 cm^{-1} spectral region. The vertical lines (top) represent the calculated first-order intensities. The spectral simulation (down) has been performed by superposing the first-, second-, and third-order spectra.

N−H waggings (especially the N1−H wagging). To explain this problem in the case of uracil, two main reasons had been invoked: (i) a strong H-bond network, which is obviously absent in the theoretical calculations performed for an isolated molecule. (ii) A strong coupling predicted by the calculations between the N1−H wagging and the skeleton torsional modes. In the case of thymine, although the crystal structures[17,18] present shorter H-bond lengths, leading to a stronger H-bond network compared to uracil, the scaled force field allowed all three N−H and C−H wagging modes to be satisfactorily assigned (Table 2, Figure 8). Thus, the absence of an H-bond in the theoretical model is not sufficient to explain the discrepancies encountered

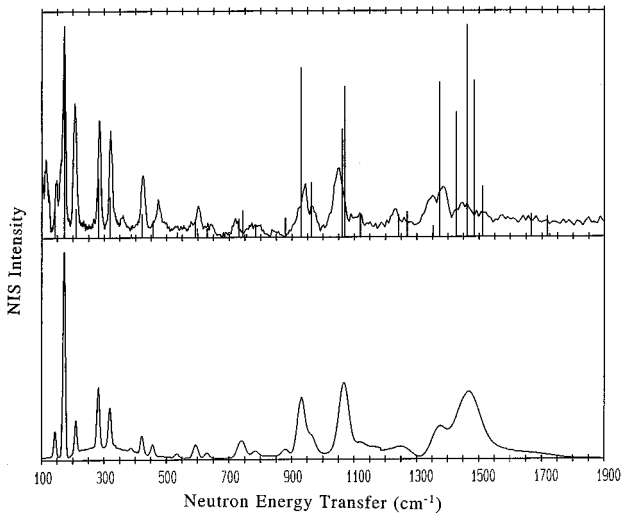

Figure 7. Comparison between experimental (top) and simulated NIS (with scaled 6-31G(*) force field) spectra for T-d_2 species in the 100−1900 cm^{-1} spectral region. See the caption of Figure 6.

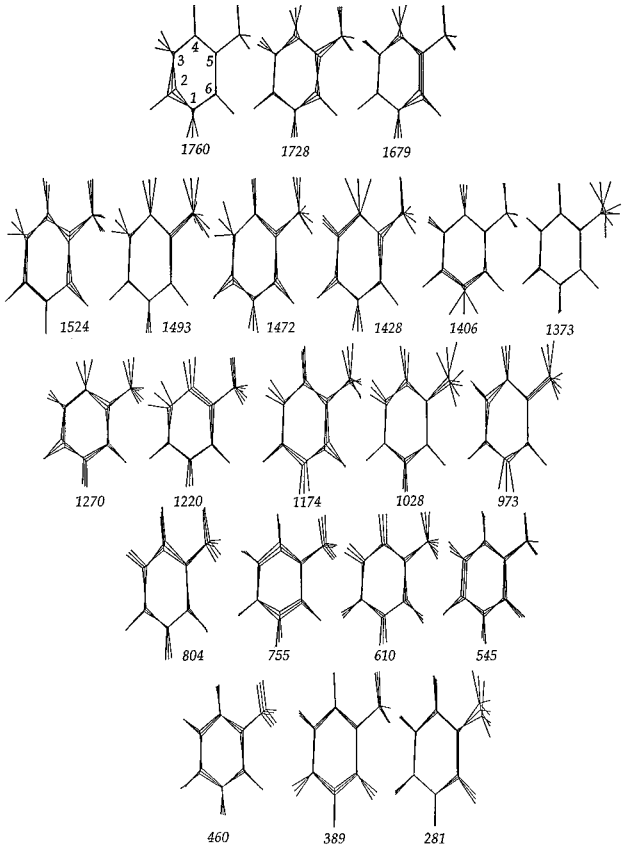

Figure 8. Graphic representation of calculated (with scaled 6-31G(*) force field) A′-symmetry vibrational modes (below 2000 cm^{-1}) of thymine. Assignments of these modes in terms of internal coordinates are reported in Table 1.

in the case of uracil. As regards the coupling between N1−H wagging and the torsional motions, some subtle differences between uracil and thymine should be emphasized here. In uracil, the calculated modes below 250 cm^{-1} provide large out-of-plane displacements of H1 atom, while in thymine similar modes mostly involve N1 and N3 out-of-plane motions (see graphical representations of 210 and 143 cm^{-1} modes in Figure 9). We conclude that the existence of the methyl group in the molecular system of thymine would significantly alter the nature of the coupling between the N−H wagging and the torsional motions. Thus, the scaling of the N−H wagging vibrations in

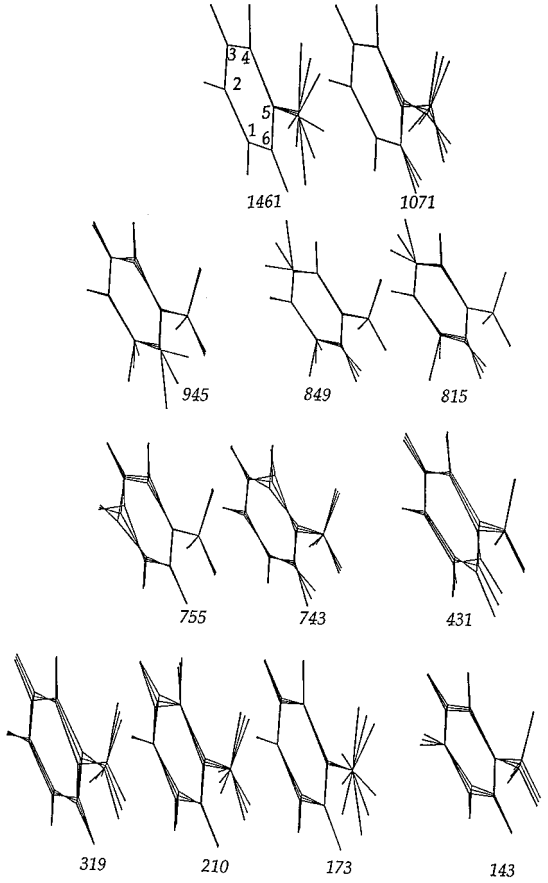

Figure 9. Graphic representation of calculated A″-symmetry vibrational modes of thymine. See the caption of Figure 8 and Table 1.

the 800−900 cm^{-1} range, becomes easier than in the case of uracil. The calculations also account for the isotopic shifts of these wagging vibrations.

In thymine, the coupling between the C5−C(H3), C6−H, and N1−H waggings gives rise to an intense NIS band at 431 cm^{-1} (432 cm^{-1} in Raman) which is shifted to 424 cm^{-1} (426 cm^{-1} in Raman) upon deuteration (Figures 2 and 3).

NIS spectra of uracil exhibit a broad gap between 250 and 400 cm^{-1}, whereas thymine yields two narrow bands at 286 and 323 cm^{-1} with a major contribution from the methyl group vibrational motions. The lack of hydrogen motions in the calculated mode at 210 cm^{-1} (observed at 206 cm^{-1} in NIS spectrum, Figure 6), leads to the underestimation of its intensity. As in the case of uracil,[1] the NIS spectral shape below 350 cm^{-1} remains unchanged upon N-deuteration: the contribution of the N−H hydrogen motions is expected to be weak. For thymine, this fact is accounted for by our calculations. The most prominent NIS band observed at 174 cm^{-1} is assigned to the methyl group torsional mode.

Finally, resolved Raman bands observed at $T = 15$ K around 129, 121, 100, 82, 47, and 36 cm^{-1} can be assigned to the lattice modes. The broadening of these bands from low to room temperature, as well as their intensity enhancement, can be observed in Figure 2.

Conclusions

Once again it has been shown that the joint use of the experimental (NIS and optical) spectra and normal mode calculations performed by means of an adequate quantum mechanical force field allows the main vibrational features of a nucleic acid base to be understood. In all previous works on thymine, even those using extended atomic basis sets and correlation effects, the theoretical assignements were based on the wavenumbers observed in IR and/or Raman spectra. Unfortunately, the low-wavenumber modes, mainly arising from the C−H and N−H waggings or from the ring torsional motions, are either not observed or are of very low intensity in optical spectra, whereas these modes give rise to very intense bands in NIS spectra. Thus, the proposition of an SQM force field for nucleic acid bases, fitted on IR, Raman, and NIS spectra, has a better chance to be realistic.

Full unscaled and scaled force constant matrixes can be provided upon request.

Acknowledgment. The authors thank the Rutherford Appleton Laboratory staff for their technical assistance in using TFXA to obtain the NIS spectra. All of the quantum chemical computations reported in this paper have been carried out on Cray C98 computers. The authors thank IDRIS (Institut du Développement et des Ressources en Informatique Scientifique, CNRS) for access to computational facilities. Many thanks to Dr. F. Romain (Laboratoire de Spectrochimie Infrarouge et Raman) for recording the Raman spectra at low temperature. A.A. is partially supported by a fellowship from the Government of Morocco.

References and Notes

(1) Aamouche, A.; Ghomi, M.; Coulombeau, C.; Jobic, H.; Grajcar, L.; Baron, M. H.; Baumruk, V.; Turpin, P. Y.; Henriet, C.; Berthier G. *J. Phys. Chem.* **1996**, *100*, 5224.

(2) Ferro, D.; Bencivenni, L.; Teghil, R.; Mastromarino, R. *Thermochim. Acta* **1980**, *42*, 75.

(3) Les, A.; Adamowicz, L.; Nowak, M. J.; Lapinski, L. *Spectrochim. Acta* **1992**, *48A*, 1385.

(4) Person, W. B.; Szczepaniak, K. In *Vibrational Spectra and Structure*; Durig, J. R., Ed.; Elsevier: Amsterdam, 1993; Vol. 20, p 239.

(5) Angell, C. L. *J. Chem. Soc.* **1961**, 504.

(6) Susi, H.; Ard, J. S. *Spectrochim. Acta* **1974**, *30A*, 1843.

(7) Florian, J.; Hrouda, V. *Spectrochim. Acta* **1993**, *49A*, 921.

(8) Rush III, T.; Peticolas, W. L. *J. Phys. Chem.* **1995**, *99*, 14647.

(9) Aamouche, A.; Berthier, G.; Coulombeau, C.; Flament, J. P.; Ghomi, M.; Henriet, C., Jobic, H.; Turpin, P. Y. *Chem. Phys.* **1996**, *204*, 353.

(10) Penfold, J.; Tomkinson, J., *Rutherford Appleton Laboratory Report;* RAL-86-019; Rutherford Appleton Laboratory: Chilton, 1988.

(11) Tomkinson, J.; Carlile, C. J.; Lovsey, S. W.; Osbora, R.; Taylor, A. D. In *Spectroscopy of Advanced Materials*; Clark, R. J. H., Hester, R. E., Eds.; John Wiley and Sons: Chichester, 1991; Chapter 3.

(12) Jobic, H.; Lauter, H. J. *J. Chem. Phys.* **1988**, *88*, 5450.

(13) Hehre, W. J., Radom, L.; Schleyer, P. v. R.; Pople, J. A. In *Ab Initio Molecular Orbital Theory*; Wiley: New York, 1986.

(14) Frisch, M., *Gaussian 90 User's Guide*; Gaussian, Inc.: Carnegie-Mellon University, 1990.

(15) Wilson Jr., E. B.; Decius, J. C.; Cross, P. C. In *Molecular Vibrations*; McGraw-Hill: New York, 1955.

(16) Mastryukov, V.; Fan, K.; Boggs, J. E. *J. Mol. Struct.* **1995**, *346*, 173.

(17) Gerdil, R. *Acta Crystal*logr. **1961**, *14*, 333.

(18) Ozeki, K; Sakabe, N.; Tanaka, J. *Acta Crystallogr.* **1969**, *B25*, 1038.

(19) Török, F.; Hegedüs, A.; Kosa, K.; Pulay, P. *J. Mol. Struct*. **1976**, *32*, 93.

(20) Fogarasi, G.; Pulay, P. In *Vibrational Spectra and Structure*; Durig, J. R., Ed.; Elsevier: Amsterdam, 1985; Vol. 14, p 125.

(21) Dhaouadi, Z.; Ghomi, M.; Coulombeau, Ce.; Coulombeau, C.; Jobic, H.; Mojzes, P.; Chinsky, L.; Turpin, P. Y. *Eur. Biophys. J.* **1993**, *22*, 225.

(22) Dhaouadi, Z.; Ghomi, M.; Austin, J. C.; Girling, R. B.; Hester, R. E.; Mojzes, P.; Chinsky, L.; Turpin, P. Y.; Coulombeau, C.; Jobic, H.; Tomkinson, J. *J. Phys. Chem.* **1993**, *97*, 1074.